JBC COMMUNICATION

Structure of the complex between calmodulin and a functional construct of eukaryotic elongation factor 2 kinase bound to an ATP-competitive inhibitor

Received for publication, April 11, 2023, and in revised form, May 6, 2023 Published, Papers in Press, May 11, 2023,
https://doi.org/10.1016/j.jbc.2023.104813

Andrea Piserchio[1], Eta A. Isiorho[2], Kevin N. Dalby[3,4,*], and Ranajeet Ghose[1,5,6,7,*]

From the [1]Department of Chemistry and Biochemistry, The City College of New York, New York, New York, USA; [2]Macromolecular Crystallization Facility, CUNY ASRC, New York, New York, USA; [3]Division of Chemical Biology and Medicinal Chemistry, and [4]Interdisciplinary Life Sciences Graduate Program, The University of Texas, Austin, Texas, USA; [5]PhD Program in Biochemistry, [6]PhD Program in Chemistry, and [7]PhD Program in Physics, The Graduate Center of CUNY, New York, New York, USA

Reviewed by members of the JBC Editorial Board. Edited by Wolfgang Peti

The calmodulin-activated α-kinase, eukaryotic elongation factor 2 kinase (eEF-2K), serves as a master regulator of translational elongation by specifically phosphorylating and reducing the ribosome affinity of the guanosine triphosphatase, eukaryotic elongation factor 2 (eEF-2). Given its critical role in a fundamental cellular process, dysregulation of eEF-2K has been implicated in several human diseases, including those of the cardiovascular system, chronic neuropathies, and many cancers, making it a critical pharmacological target. In the absence of high-resolution structural information, high-throughput screening efforts have yielded small-molecule candidates that show promise as eEF-2K antagonists. Principal among these is the ATP-competitive pyrido-pyrimidinedione inhibitor, A-484954, which shows high specificity toward eEF-2K relative to a panel of "typical" protein kinases. A-484954 has been shown to have some degree of efficacy in animal models of several disease states. It has also been widely deployed as a reagent in eEF-2K-specific biochemical and cell-biological studies. However, given the absence of structural information, the precise mechanism of the A-484954-mediated inhibition of eEF-2K has remained obscure. Leveraging our identification of the calmodulin-activatable catalytic core of eEF-2K, and our recent determination of its long-elusive structure, here we present the structural basis for its specific inhibition by A-484954. This structure, which represents the first for an inhibitor-bound catalytic domain of a member of the α-kinase family, enables rationalization of the existing structure–activity relationship data for A-484954 variants and lays the groundwork for further optimization of this scaffold to attain enhanced specificity/potency against eEF-2K.

Eukaryotic elongation factor 2 kinase (eEF-2K) is an atypical serine/threonine kinase that is activated by calmodulin (CaM) (1–4) and is one of six members of the α-kinase family encoded in the human genome (5, 6). eEF-2K plays a critical role in regulating the elongation stage of translation by phosphorylating its only currently validated cellular target, the ribosome-associated guanosine triphosphatase (GTPase), eukaryotic elongation factor 2 (eEF-2) (7) that facilitates translocation of the nascent chain from the ribosomal aminoacyl site (A-site) to the peptidyl site (P-site) to accommodate an incoming aminoacyl-tRNA during elongation. The eEF-2K-mediated phosphorylation of eEF-2 on a specific threonine residue (Thr-56) compromises its ability to engage the ribosome and leads to a global downregulation of elongation (7–9) with differential effects on the translation of specific mRNA messages (10). Dysregulation of eEF-2K has been implicated in a variety of human disorders, including those of the cardiovascular system (11) and chronic neuropathies such as Alzheimer's (12) and Parkinson's (13) diseases. Aberrant eEF-2K activity has also been linked to the progression of many forms of cancer, including medulloblastoma (14), neuroblastoma (15), and breast cancer (16). Given its functional correlation with diverse disease states, eEF-2K has been recognized as a potential therapeutic target for a range of cardiovascular diseases (17), neurological conditions (18) and several cancers (19).

For several years, there have been consistent efforts to discover specific modulators of eEF-2K function (20–22). Among these, the pyrido-pyrimidinedione inhibitor, A-484954 (Fig. 1*A*), discovered through high-throughput screening, is the best-established eEF-2K inhibitor (20) that has been widely deployed in a variety of functional and *in vivo* studies. Although the potency of this inhibitor (20, 21) is modest in pharmacological terms, it has shown some efficacy in animal models of Alzheimer's disease (23), Dravet syndrome (24) and hypertension (25). Although individually these studies should be interpreted with caution since off-target effects are possible, they collectively suggest that the A-484954 scaffold may lend to further optimization for more efficiently targeting eEF-2K.

The rational design of small molecules antagonists of eEF-2K activity, or its interactions with CaM, a critical step in activation (26), had thus far been hindered by the absence of a three-dimensional structure of this enzyme or a functional construct thereof. To elucidate the mechanism of the CaM-mediated activation of eEF-2K and provide a structural framework for

* For correspondence: Ranajeet Ghose, rghose@ccny.cuny.edu; Kevin N. Dalby, dalby@austin.utexas.edu.

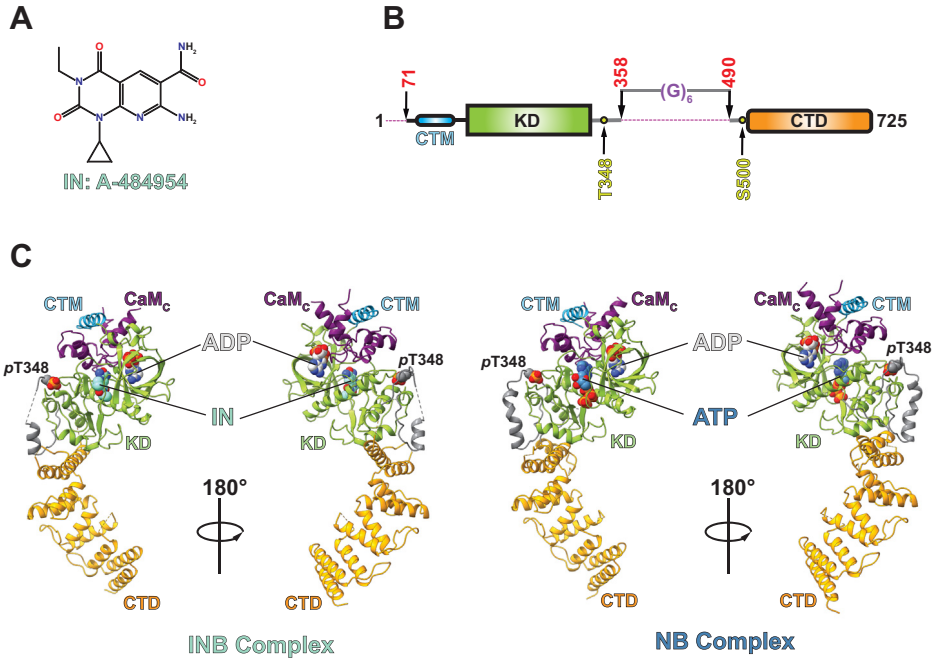

Figure 1. The inhibitor-bound CaM•*p*eEF-2K$_{TR}$ complex. *A*, chemical structure of the eEF-2K inhibitor, A-484954 (IN). *B*, schematic representation of the eEF-2K$_{TR}$ construct, showing the calmodulin-targeting motif (CTM, *blue*), the α-kinase domain (KD, *lime*), and the C-terminal domain (CTD, *orange*). The eEF-2K$_{TR}$ construct is missing (indicated by the *dashed lines*) the first 70 N-terminal residues (S70 is restored as the remnant of an affinity tag), and a portion of the regulatory loop (R-loop, 359–489) but includes the sites of primary (T348) and secondary (S500) activating autophosphorylation therein. *C*, the structure of the CaM•*p*eEF-2K$_{TR}$ complex bound to ADP and IN (INB complex) is shown on the *left panel*. Also shown for comparison in the same orientation, on the *right panel*, is the NB structure (bound to ADP and ATP; PDB: 8FNY). The various domains have been colored as in (*B*). Only the C-lobe of calmodulin (*colored purple*) within the INB and NB complexes could be modeled. The phosphorylated T348 residue (*p*T348) is also indicated.

rational drug design, we engineered a minimal CaM-activatable construct representing the functional core of eEF-2K (eEF-2K$_{TR}$, Fig. 1*B*) (27). We subsequently determined the crystal structure of the complex of eEF-2K$_{TR}$ phosphorylated at the primary activating site, T348, with CaM (CaM•*p*eEF-2K$_{TR}$) (28). As a necessary next step in designing and optimizing highly potent and selective ATP-competitive eEF-2K inhibitors, here we present the structural basis for its inhibition by A-484954. We expect that our structure, the first of an inhibitor-bound α-kinase catalytic domain, will lay the groundwork for future efforts in the rational design of antagonists targeting the active site of eEF-2K.

Results and discussion

To establish the mode of nucleotide recognition by eEF-2K, we had previously determined the structure of the CaM•*p*eEF-2K$_{TR}$ complex bound to ATP and ADP (NB, for nucleotide-bound). In the NB structure, ATP was bound at the kinase active site, while ADP was unexpectedly engaged to a basic pocket (BP) at the interface between the C-lobe of CaM (CaM$_C$) and the N-lobe of the kinase domain (KD) (Fig. 1*C*) (29). Using conditions similar to those used for the NB complex, we crystallized and solved the structure of the CaM•*p*eEF-2K$_{TR}$ complex bound to A-484954 and ADP (INB for inhibitor-bound; Fig. 1*C*).

In the INB structure (see Table S1 for details about data collection, structure refinement, and statistics), ADP is bound at the BP in a conformation identical to that seen in the NB complex (29). The inhibitor, A-484954, replaces ATP at the kinase active site (compare the left and right panels of Fig. 1*C*). The functional implications of the engagement of ADP at the BP and the resultant enhancement in the CaM-mediated activation of eEF-2K were discussed at length previously (29) and are therefore not revisited here. In the NB structure, A-484954 is stabilized at the kinase active site (Fig. S1) through numerous interactions reflective of its sub-μM IC$_{50}$ (20, 21) in an alignment such that its pyridine ring is in an equivalent spatial position to the imidazole ring of ATP (Fig. 2*A*). The sidechain of K170, which engages the adenine N$_7$ of ATP in the NB complex, now forms a hydrogen bond with the 4-oxo moiety of the dioxopyrimidine ring of the inhibitor. The carboxamide moiety is oriented through several hydrogen bonds involving the H230 and I232 backbones and the E229 sidechain (Fig. 2*B*, top left). These residues are also involved in the recognition of ATP in the NB complex, with the adenine N$_6$ forming hydrogen bonds with the sidechain and mainchain of E229 and H230, respectively, while N$_1$ engages the I232 mainchain (Fig. 2*B*, top right). The Y236 ring takes part in π-π stacking interactions with the dioxopyrimidine ring of the inhibitor (Fig. 2*B*, bottom left), substituting a corresponding stacking with the adenine ring of ATP in the NB complex, albeit with a slightly altered geometry (Fig. 2*B*, bottom right). This interaction is supplemented by a donor-π interaction (30) with C146 (Fig. 2*B*, top left) and hydrophobic contacts with V168 (Fig. 2*B*, bottom left). In contrast, the ethyl and

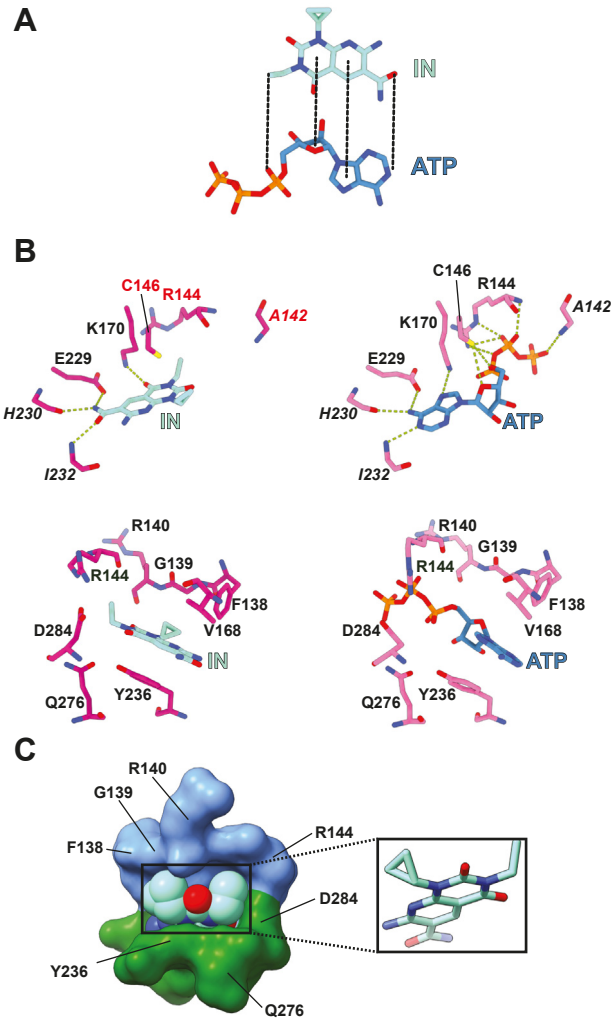

Figure 2. The inhibitor occupies the active site of *pe*EF-2K$_{TR}$. *A*, comparison of the spatial positioning of A-484954 (in the INB complex) with respect to ATP (in the NB complex; PDB: 8FNY) at the *pe*EF-2K$_{TR}$ active site. The dashed vertical lines indicate equivalent spatial positions. The pyridine ring of the inhibitor occupies the same spatial position as the imidazole ring of ATP. *B*, hydrogen-bonding patterns (*top*) and other key contacts (*bottom*) are shown for A-484954 (*left*) and ATP (*right*) in the INB and NB complexes, respectively. Residues that form hydrogen bonds (*green dashed lines*) using only their backbone atoms are indicated in italicized font. Hydrogen bonds involving A142, R144, and C146 with ATP seen in the NB complex are missing in the INB complex. These residues are labeled in red font on the *top left panel*. Note that the NB structure has two molecules in the asymmetric unit. The two protomers have subtle differences in the orientations of the triphosphate moieties of ATP (given the absence of essential Mg^{2+} ions in the structure). This leads to small differences in the corresponding hydrogen bonding networks (29). The ATP molecule bound to chain A is shown here. Hydrogen bonds were calculated using UCSF ChimeraX (49) by relaxing constraints by 0.5 Å and 20°. The π-stacking interactions of Y236 (*bottom panel*) are somewhat different between A-484954 and ATP. The inter-centroid distance and interplanar angle between Y236 and the dioxopyrimidine ring of the inhibitor are 4.0 Å and 14.2°, respectively; the corresponding values with the imidazole ring of ATP are 4.9 Å and 27.3°. *C*, van der Waals contacts of A-484954 bound at the *pe*EF-2K$_{TR}$ active site. The local surface encompassing key kinase residues that contact the cyclopropyl and the ethyl moieties of A-484954 is shown. Elements corresponding to the N- and C-lobes of the kinase domain are colored blue and green, respectively. The inset illustrates the orientation of the inhibitor in the kinase active site in this view.

cyclopropyl moieties of the inhibitor show few specific, directional contacts with the kinase. However, several van der Waals contacts of the cyclopropyl ring with F138, G139, and R140, and the ethyl group with R144, Q276, and D284, are seen. Y236 contacts both the cyclopropyl and the ethyl moieties of the inhibitor. These non-specific interactions appear to be important since significant modifications of the ethyl or the cyclopropyl groups significantly weaken binding (21). We suspect these contacts are important to stabilize a relatively close-packed structure at the entrance to the kinase active site (Fig. 2*C*). Consistent with the structure presented here, the replacement of the ethyl moiety by smaller entities (a hydrogen or a methyl group), that would result in reduced packing, lead to ∼15-fold increases in the IC_{50}. While replacement with a slightly larger propyl moiety is tolerated (∼2-fold increase in the IC_{50}), introducing a significantly bulkier group, for example, CH_2-Ph-NH_2, that would require more substantial conformational rearrangements to prevent steric clashes, results in a >50-fold increase in IC_{50}. The importance of the hydrogen bonds involving the carboxamide moiety, discussed above, is also evident since even minor changes, for example, the replacement of the oxygen with sulfur, result in a >50-fold increase in IC_{50} (21).

We have previously noted a closure of the phosphate-binding P-loop relative to the N/D-loop in *pe*EF-2K$_{TR}$ upon comparing the NB structure with that in the absence of nucleotides (nucleotide-free, NF) (29). A comparison of the NB and INB structures suggests a further closure of the P-loop upon replacing ATP with A-484954 at the kinase active site (Fig. 3*A*). It is notable that F138, G139, R140, and R144, mentioned above, are all part of the P-loop on the N-lobe of the kinase, while Y236, Q276, and D284 are housed on the C-lobe (Fig. 2*C*). Therefore, it appears that the ethyl and cyclopropyl groups on A-484954 serve to bridge the N- and C-lobes of the kinase domain and stabilize a closed state. This enhanced degree of closure appears to be a common feature in nucleotide-bound α-kinases KDs (29, 31).

In addition to the relatively modest differences at/near the active site between the NB and INB structures, substantial differences are noted at a distance more than 35 Å away from the catalytic center. In the NF and NB structures, the A501-N510 segment at the N-terminal end of the C-terminal domain folds into a helix (α1′; secondary structural elements as defined by Piserchio *et al.* (28)). This element is absent in the INB structure, in which the entire segment extending to K516 could not be modeled due to weak/missing density. In contrast to the NF and NB structures, the N-terminus of the subsequent helix (α2′) is lengthened by a single turn in the INB structure. We also obtained a second inhibitor-bound structure (INB2, see Table S2 for data collection, structure refinement, and statistics) that shows density suggesting partial occupancies of both these conformations, that is, the presence of α1′ and a longer α2′ (Figs. 3*B* and S2). This indicates significant conformational heterogeneity around a region proximal to S500, a site of activating autophosphorylation (32) also targeted by PKA (33). Perhaps disorder in this region, a feature likely to be enhanced by an intact R-loop (absent in eEF-2K$_{TR}$; see Fig. 1*B*), is necessary to facilitate phosphorylation on S500. It is also possible that this conformational variability is an artifact of the R-loop truncation used to generate eEF-2K$_{TR}$.

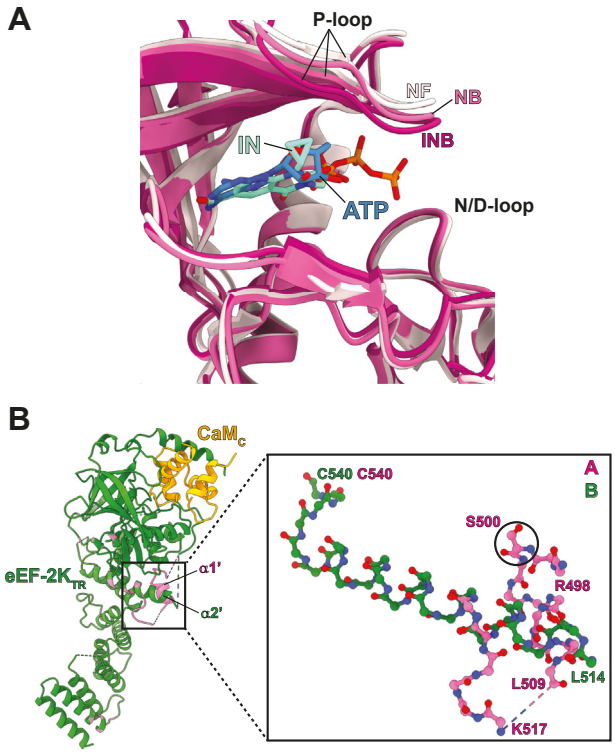

Figure 3. Conformational variability in the inhibitor-bound complex. *A*, Comparison of the relative conformations of the P- and N/D-loops in the nucleotide-free (NF; *light pink*; PDB: 7SHQ), nucleotide bound (NB; *dark pink*; PDB: 8FNY), and inhibitor-bound (INB; *magenta*) complexes. The ATP (*blue*) and A-484954 (IN, *cyan*) molecules are shown in stick representation. *B*, structure of the INB2 complex, *pe*EF-2K$_{TR}$, is shown in magenta for conformation *A*, and *green* for conformation *B*; CaM is in *orange* (only CaM$_C$ is resolved in the complex). The *right panel* shows an expansion of the variable region in ball and stick representation. S500, which is only visible in conformation *A*, is circled. The termini of the segments represented for the two conformations are labeled. The features corresponding to conformation *A* are seen in the NF and NB complexes, while those corresponding to conformation *B* are seen in the INB complex.

Notably, while the CaM-driven autophosphorylation at the primary activating site, T348, is rapid, we have been unable to detect autophosphorylation on S500 in eEF-2K$_{TR}$ even after an hour of incubation with ATP and Mg^{2+}. The overall orientations of the inhibitor bound at the eEF-2K$_{TR}$ active site are indistinguishable between the INB and INB2 structures (Fig. S3).

A-484954 has been suggested to be highly specific for eEF-2K and inactive "against a wide panel of serine/threonine and tyrosine kinases" (20). To understand the origin of this selectivity, we compared the structure of eEF-2K$_{TR}$ with PKA and the kinases included in the screen to determine residues that are spatially equivalent to those (C146, V168, K170, E229, and Y236; see Table S3 for a representative subset) whose sidechains appear to be involved in A-484954 recognition. Of these residues, only the "catalytic lysine" K170 seems common within this group. In conventional kinases (K72 in PKA; Table S3), this residue forms a critical salt bridge with a conserved glutamate (E91 in PKA) on the αC helix to maintain an "αC in" conformation and correctly position the α– and β–phosphates of ATP in the active state (34). The positions equivalent to C146 (V57 in PKA) and V168 (A70) comprise key hydrophobic components of the so-called catalytic spine (C-spine) in conventional kinases (35, 36). The spatial position of E229 corresponds to that of the so-called gatekeeper (37, 38), generally a bulky hydrophobic residue in most conventional kinases. Finally, the position corresponding to Y236 is never aromatic in the conventional kinases used in the panel (20). Based on this simple analysis, it appears unlikely that the critical interactions that stabilize A-484954 within the eEF-2K active site can be recapitulated in the active sites of conventional protein kinases, reflective of its previously-determined selectivity towards eEF-2K (20).

In contrast to the conventional kinases, eEF-2K residues that engage A-484954 show a high degree of conservation among human α-kinases, with K170 and E229 being invariant in all α-kinases (39). The other critical positions are also quite similar in human α-kinases. V168 is a valine in ALPK1 and ALPK2, and isoleucine in ALPK3, TRPM6 and TRPM7. Y236 is a phenylalanine in ALPK1, ALPK2, TRPM6, and TRPM7, except in ALPK3, where it is a leucine, potentially substituting the π-π stacking seen in eEF-2K by a methyl-π interaction. Based on these observations, whether A-484594 would provide sufficient specificity towards eEF-2K over the other five human α-kinases is unclear. However, the position corresponding to C146, an alanine in the other five human α-kinases, is distinct in eEF-2K (6). This residue could perhaps provide a means to enhance specificity and potency through reversible covalent targeting. For example, the cysteine Sγ atom is less than 5 Å away from both the ethyl and the cyclopropane moieties of A-484954. A previous study employing carbonitrile-based inhibitors in eEF-2K indicated that the C146 sidechain could be covalently targeted (40). However, careful thought is required for designing and placing such a modifier on the A-484954 scaffold since the donor-π interaction involving C146, mentioned earlier, could potentially affect its reactivity. Nevertheless, we expect that the present structure, the first of an inhibitor-bound eEF-2K, and indeed of any α-kinase bound to an inhibitor, will provide a framework for the rational design of ATP-competitive antagonists targeting this critical regulator of translational elongation.

Experimental procedures

Crystallization

CaM and *pe*EF-2K$_{TR}$ were expressed and purified, and their 1:1 complex was generated as described previously (28). For crystallization, the CaM•*pe*EF-2K$_{TR}$ complex prepared in buffer containing 20.0 mM Tris (pH 7.5), 100.0 mM NaCl, 3.0 mM $CaCl_2$, 1.0 mM TCEP was concentrated to 10.3 mg/ml using a spin column (Amicon Ultra, Millipore) with a 3.0 kDa cutoff. The ligand stock solution comprising 44.4 mM A-484954 (TargetMol, Catalog number: TQ0137) dissolved in ^{2}H-DMSO was added immediately before plating to the protein solution at concentrations of 0.3 mM (~0.7% ^{2}H-DMSO) or 1.5 mM (~3.1% ^{2}H-DMSO), together with 0.3 mM ADP and 1.5 mM $MgCl_2$. Under these conditions, the presence of ADP in the buffer was essential for the success of the co-crystallization experiments. Optimal crystallization conditions were

established by simultaneous application of PEG-3350 (Hampton Research, 12 steps from 16% to 22%) and pH gradients (8 steps from 5.9 to 7.0, or from 6.5 to 8.5) in the presence of 100.0 mM Bis-Tris Propane and 200.0 mM NaF (Hampton Research) using Art-Robbins low profile, 3-well Intelli-Plate 96 plates. The crystallization cocktails were prepared using an SPT Labtech Dragonfly liquid handling robot and mixed with the protein stock in ratios of 2:1, 1:1, and 1:2 (0.2 μl total volume) using an SPT Labtech Mosquito. The structures presented in this study were derived from crystals obtained from a batch (two parts) containing 0.3 mM inhibitor, ∼0.7% ^{2}H-DMSO, mixed with a cocktail containing 16.5% PEG-3350, pH 6.2 (one part); and a batch (two parts) containing 1.5 mM inhibitor, 3.1% ^{2}H-DMSO, mixed with 16.5% PEG-3350, pH 6.5 (one part). These crystals were looped directly from the Intelli-Plate wells, cryoprotected with LV CryoOil (Mitegen), and stored in liquid N_2 before data collection.

Data collection and structure determination

Diffraction data were acquired on the FMX beamline at NSLS-II and processed using the autoPROC toolbox (41). Phases were obtained by molecular replacement and our initial structure of the CaM•*p*eEF-2K$_{TR}$ complex (PDB: 7SHQ) (28) using Phaser after removing the N-lobe of CaM, and refined using phenix.refine (42, 43). The ligands, ADP and A-484954, were prepared using eLBOW (44) and fitted using phenix.ligandfit (45, 46). The metal ions were assigned using the CheckMyBlob server (47). The first dataset, truncated with a spherical cutoff (2.009 Å), was initially refined at 2.327 Å. The resolution limit was extended to 2.120 Å using PAIRREF (48) following prescribed guidelines, with a visual inspection of the $2F_O$-F_C map in the region around the bound A-484954. The second dataset (corresponding to INB2) was refined with data integrated using an ellipsoidal shell, as previously described (29).

Data availability

Structure factors and atomic coordinates have been deposited in the Protein Data Bank with PDB IDs 8GM4 and 8GM5.

Supporting information—This article contains supporting information (20, 35, 37, 49, 50).

Author contributions—A. P. investigation; A. P. and E. A. I investigation and formal analysis; K. N. D. and R. G. conceptualization, supervision, and resources; R. G. writing – original draft; A. P., E. A. I., K. N. D. and R. G. writing – review and editing.

Funding and additional information—This work is supported by NIH award R01 GM123252 (to K. N. D. and R. G.) and a CPRIT award RP210088 (to K. N. D.). Use of the NYX beamline (19-ID) at the National Synchrotron Light Source II (NSLS-II) is supported by the member institutions of the New York Structural Biology Center. NSLS-II is a United States Department of Energy (DOE) Office of Science user facility operated for the DOE Office of Science by Brookhaven National Laboratory under Contract DE-SC0012704. Dr Kevin Battaile (New York Structural Biology Center) and Dr Dale Kreitler (NSLS-II) are thanked for their support during data collection and analysis.

Conflict of interest—The authors declare that they have no conflicts of interest with the contents of this article.

Abbreviations—The abbreviations used are: BP, basic pocket; CAM_c, C-lobe of CaM; CaM, calmodulin; eEF-2K, Eukaryotic elongation factor 2 kinase; eEF-2, eukaryotic elongation factor 2; GTPase, guanosine triphosphatase; KD, kinase domain; NB, nucleotide-bound.

References

1. Nairn, A. C., Bhagat, B., and Palfrey, H. C. (1985) Identification of calmodulin-dependent protein kinase III and its major M_r 100,000 substrate in mammalian tissues. *Proc. Natl. Acad. Sci. U. S. A.* **82**, 7939–7943
2. Nairn, A. C., and Palfrey, H. C. (1987) Identification of the major M_r 100,000 substrate for calmodulin-dependent protein kinase III in mammalian cells as elongation factor-2. *J. Biol. Chem.* **262**, 17299–17303
3. Ryazanov, A. G. (1987) Ca^{2+}/calmodulin-dependent phosphorylation of elongation factor 2. *FEBS Lett.* **214**, 331–334
4. Ryazanov, A. G., Natapov, P. G., Shestakova, E. A., Severin, F. F., and Spirin, A. S. (1988) Phosphorylation of the elongation factor 2: the fifth Ca^{2+}/calmodulin-dependent system of protein phosphorylation. *Biochimie* **70**, 619–626
5. Drennan, D., and Ryazanov, A. G. (2004) Alpha-kinases: analysis of the family and comparison with conventional protein kinases. *Prog. Biophys. Mol. Biol.* **85**, 1–32
6. Middelbeek, J., Clark, K., Venselaar, H., Huynen, M. A., and van Leeuwen, F. N. (2010) The alpha-kinase family: an exceptional branch on the protein kinase tree. *Cell. Mol. Life Sci.* **67**, 875–890
7. Ryazanov, A. G., Shestakova, E. A., and Natapov, P. G. (1988) Phosphorylation of elongation factor 2 by EF-2 kinase affects rate of translation. *Nature* **334**, 170–173
8. Ryazanov, A. G., and Davydova, E. K. (1989) Mechanism of elongation factor 2 (EF-2) inactivation upon phosphorylation. Phosphorylated EF-2 is unable to catalyze translocation. *FEBS Lett.* **251**, 187–190
9. Carlberg, U., Nilsson, A., and Nygard, O. (1990) Functional properties of phosphorylated elongation factor 2. *Eur. J. Biochem.* **191**, 639–645
10. Sossin, W. S., and Costa-Mattioli, M. (2019) Translational control in the brain in health and disease. *CSH Persp. Biol.* **11**, a032912
11. Usui, T., Okada, M., Hara, Y., and Yamawaki, H. (2013) Eukaryotic elongation factor 2 kinase regulates the development of hypertension through oxidative stress-dependent vascular inflammation. *Am. J. Physiol. Heart Circ. Physiol.* **305**, H756–768
12. Yang, W., Zhou, X., Ryazanov, A. G., and Ma, T. (2021) Suppression of the kinase for elongation factor 2 alleviates mGluR-LTD impairments in a mouse model of Alzheimer's disease. *Neurobiol. Aging* **98**, 225–230
13. Jan, A., Jansonius, B., Delaidelli, A., Bhanshali, F., An, Y. A., Ferreira, N., *et al.* (2018) Activity of translation regulator eukaryotic elongation factor-2 kinase is increased in Parkinson disease brain and its inhibition reduces alpha synuclein toxicity. *Acta Neuropathol. Commun.* **6**, 54
14. Leprivier, G., Remke, M., Rotblat, B., Dubuc, A., Mateo, A. R., Kool, M., *et al.* (2013) The eEF2 kinase confers resistance to nutrient deprivation by blocking translation elongation. *Cell* **153**, 1064–1079
15. Delaidelli, A., Negri, G. L., Jan, A., Jansonius, B., El-Naggar, A., Lim, J. K. M., *et al.* (2017) *MYCN* amplified neuroblastoma requires the mRNA translation regulator eEF2 kinase to adapt to nutrient deprivation. *Cell Death Differ.* **24**, 1564–1576
16. Meric-Bernstam, F., Chen, H., Akcakanat, A., Do, K. A., Lluch, A., Hennessy, B. T., *et al.* (2012) Aberrations in translational regulation are associated with poor prognosis in hormone receptor-positive breast cancer. *Breast Cancer Res.* **14**, R138

17. Zhang, P., Riazy, M., Gold, M., Tsai, S. H., McNagny, K., Proud, C., *et al.* (2014) Impairing eukaryotic elongation factor 2 kinase activity decreases atherosclerotic plaque formation. *Can. J. Cardiol.* **30**, 1684–1688
18. Beretta, S., Gritti, L., Verpelli, C., and Sala, C. (2020) Eukaryotic elongation factor 2 kinase a pharmacological target to regulate protein translation dysfunction in neurological diseases. *Neuroscience* **445**, 42–49
19. Temme, L., and Asquith, C. R. M. (2021) eEF2K: an atypical kinase target for cancer. *Nat. Rev. Drug Discov.* **20**, 577
20. Chen, Z., Gopalakrishnan, S. M., Bui, M. H., Soni, N. B., Warrior, U., Johnson, E. F., *et al.* (2011) 1-Benzyl-3-cetyl-2-methylimidazolium iodide (NH125) induces phosphorylation of eukaryotic elongation factor-2 (eEF2): a cautionary note on the anticancer mechanism of an eEF2 kinase inhibitor. *J. Biol. Chem.* **286**, 43951–43958
21. Edupuganti, R., Wang, Q., Tavares, C. D., Chitjian, C. A., Bachman, J. L., Ren, P., *et al.* (2014) Synthesis and biological evaluation of pyrido[2,3-d] pyrimidine-2,4-dione derivatives as eEF-2K inhibitors. *Bioorg. Med. Chem.* **22**, 4910–4916
22. Klupt, K. A., and Jia, Z. (2023) eEF2K Inhibitor design: the progression of exemplary structure-based drug design. *Molecules* **28**, 1095
23. Kasica, N. P., Zhou, X., Yang, Q., Wang, X., Yang, W., Zimmermann, H. R., *et al.* (2022) Antagonists targeting eEF2 kinase rescue multiple aspects of pathophysiology in Alzheimer's disease model mice. *J. Neurochem.* **160**, 524–539
24. Beretta, S., Gritti, L., Ponzoni, L., Scalmani, P., Mantegazza, M., Sala, M., *et al.* (2022) Rescuing epileptic and behavioral alterations in a Dravet syndrome mouse model by inhibiting eukaryotic elongation factor 2 kinase (eEF2K). *Mol. Autism* **13**, 1
25. Kodama, T., Okada, M., and Yamawaki, H. (2020) Eukaryotic elongation factor 2 kinase inhibitor, A484954 lowered blood pressure in spontaneously hypertensive rats *via* inducing vasorelaxation. *J. Pharmacol. Sci.* **144**, 165–171
26. Tavares, C. D., Ferguson, S. B., Giles, D. H., Wang, Q., Wellmann, R. M., O'Brien, J. P., *et al.* (2014) The molecular mechanism of eukaryotic elongation factor 2 kinase activation. *J. Biol. Chem.* **289**, 23901–23916
27. Will, N., Lee, K., Hajredini, F., Giles, D. H., Abzalimov, R. R., Clarkson, M., *et al.* (2018) Structural dynamics of the activation of elongation factor 2 kinase by Ca^{2+}-calmodulin. *J. Mol. Biol.* **430**, 2802–2821
28. Piserchio, A., Isiorho, E. A., Long, K., Bohanon, A. L., Kumar, E. A., Will, N., *et al.* (2022) Structural basis for the calmodulin-mediated activation of eukaryotic elongation factor 2 kinase. *Sci. Adv.* **8**, eabo2039
29. Piserchio, A., Long, K. J., Browning, L. S., Bohanon, A. L., Isiorho, E. A., Dalby, K. N., *et al.* (2023) ADP enhances the allosteric activation of eukaryotic elongation factor 2 kinase by calmodulin. *Proc. Natl. Acad. Sci. U. S. A.* **120**, e2300902120
30. Forbes, C. R., Sinha, S. K., Ganguly, H. K., Bai, S., Yap, G. P., Patel, S., *et al.* (2017) Insights into thiol-aromatic interactions: A stereoelectronic basis for S-H/π interactions. *J. Am. Chem. Soc.* **139**, 1842–1855
31. Ye, Q., Yang, Y., van Staalduinen, L., Crawley, S. W., Liu, L., Brennan, S., *et al.* (2016) Structure of the *Dictyostelium* myosin-II heavy chain kinase A (MHCK-A) alpha-kinase domain apoenzyme reveals a novel autoinhibited conformation. *Sci. Rep.* **6**, 26634
32. Tavares, C. D., O'Brien, J. P., Abramczyk, O., Devkota, A. K., Shores, K. S., Ferguson, S. B., *et al.* (2012) Calcium/calmodulin stimulates the autophosphorylation of elongation factor 2 kinase on Thr-348 and Ser-500 to regulate its activity and calcium dependence. *Biochemistry* **51**, 2232–2245
33. Redpath, N. T., and Proud, C. G. (1993) Cyclic AMP-dependent protein kinase phosphorylates rabbit reticulocyte elongation factor-2 kinase and induces calcium-independent activity. *Biochem. J.* **293**, 31–34
34. Modi, V., and Dunbrack, R. L., Jr. (2019) Defining a new nomenclature for the structures of active and inactive kinases. *Proc. Natl. Acad. Sci. U. S. A.* **116**, 6818–6827
35. Kornev, A. P., Haste, N. M., Taylor, S. S., and Eyck, L. F. (2006) Surface comparison of active and inactive protein kinases identifies a conserved activation mechanism. *Proc. Natl. Acad. Sci. U. S. A.* **103**, 17783–17788
36. Kornev, A. P., and Taylor, S. S. (2010) Defining the conserved internal architecture of a protein kinase. *Biochim. Biophys. Acta* **1804**, 440–444
37. Liu, Y., Shah, K., Yang, F., Witucki, L., and Shokat, K. M. (1998) A molecular gate which controls unnatural ATP analogue recognition by the tyrosine kinase v-Src. *Bioorg. Med. Chem.* **6**, 1219–1226
38. Taylor, S. S., and Kornev, A. P. (2011) Protein kinases: evolution of dynamic regulatory proteins. *Trends Biochem. Sci.* **36**, 65–77
39. Ye, Q., Crawley, S. W., Yang, Y., Cote, G. P., and Jia, Z. (2010) Crystal structure of the alpha-kinase domain of *Dictyostelium* myosin heavy chain kinase A. *Sci. Signal.* **3**, ra17
40. Devkota, A. K., Edupuganti, R., Yan, C., Shi, Y., Jose, J., Wang, Q., *et al.* (2014) Reversible covalent inhibition of eEF-2K by carbonitriles. *ChemBioChem* **15**, 2435–2442
41. Vonrhein, C., Flensburg, C., Keller, P., Sharff, A., Smart, O., Paciorek, W., *et al.* (2011) Data processing and analysis with the autoPROC toolbox. *Acta Crystallogr. D Biol. Crystallogr.* **67**, 293–302
42. Afonine, P. V., Grosse-Kunstleve, R. W., Echols, N., Headd, J. J., Moriarty, N. W., Mustyakimov, M., *et al.* (2012) Towards automated crystallographic structure refinement with phenix.refine. *Acta Crystallogr. D Biol. Crystallogr.* **68**, 352–367
43. Zwart, P. H., Afonine, P. V., Grosse-Kunstleve, R. W., Hung, L. W., Ioerger, T. R., McCoy, A. J., *et al.* (2008) Automated structure solution with the PHENIX suite. *Meth. Mol. Biol.* **426**, 419–435
44. Moriarty, N. W., Grosse-Kunstleve, R. W., and Adams, P. D. (2009) Electronic Ligand Builder and Optimization Workbench (eLBOW): a tool for ligand coordinate and restraint generation. *Acta Crystallogr. D Biol. Crystallogr.* **65**, 1074–1080
45. Terwilliger, T. C., Adams, P. D., Moriarty, N. W., and Cohn, J. D. (2007) Ligand identification using electron-density map correlations. *Acta Crystallogr. D Biol. Crystallogr.* **63**, 101–107
46. Terwilliger, T. C., Klei, H., Adams, P. D., Moriarty, N. W., and Cohn, J. D. (2006) Automated ligand fitting by core-fragment fitting and extension into density. *Acta Crystallogr. D Biol. Crystallogr.* **62**, 915–922
47. Brzezinski, D., Porebski, P. J., Kowiel, M., Macnar, J. M., and Minor, W. (2021) Recognizing and validating ligands with CheckMyBlob. *Nucl. Acids Res.* **49**, W86–W92
48. Maly, M., Diederichs, K., Dohnalek, J., and Kolenko, P. (2020) Paired refinement under the control of PAIREF. *IUCrJ* **7**, 681–692
49. Pettersen, E. F., Goddard, T. D., Huang, C. C., Meng, E. C., Couch, G. S., Croll, T. I., *et al.* (2021) UCSF ChimeraX: structure visualization for researchers, educators, and developers. *Protein Sci.* **30**, 70–82
50. Liebschner, D., Afonine, P. V., Moriarty, N. W., Poon, B. K., Sobolev, O. V., Terwilliger, T. C., *et al.* (2017) Polder maps: improving OMIT maps by excluding bulk solvent. *Acta Crystallogr. D Struct. Biol.* **73**, 148–157